Uniqueness Domains of Offset Wrist Robots via a 4D Workspace Representation

Alexander Feeß and Martin G. Weiß

Abstract We present a new method for studying the workspace of 6R robots using a 4D representation. This is applied to numerically determine connected workspace components with a constant number of solutions to the inverse kinematics, and to describe critical values that form the boundaries to these regions. To define and maximize uniqueness domains, nonsingular transitions between these components are investigated. This provides a method to determine workspace regions in which the robot can move avoiding configuration changes and singularities.

1 Introduction

Most established 6R robots rely on special structures that result in simplified kinematic properties, such as a decoupling of positional and orientational components [8]. This results in up to 8 inverse kinematics solutions (IKS) for each target pose. Moreover, these IKS are separated by singularities. Therefore, removing the singularity set groups the remaining joint configurations into 8 *uniqueness domains*, i.e., connected sets containing at most one IKS for any given target.

Robots with offset wrist posses kinematic properties of increased complexity. One particular observation is the possibility to change between some of the IKS via a nonsingular motion. A more problematic effect is the existence of interior singularities that manifest as workspace boundaries. These behave

A. Feeß
OTH Regensburg, Germany
e-mail: alexander.feess@oth-regensburg.de

M. G. Weiß
OTH Regensburg, Germany
e-mail: martin.weiss@oth-regensburg.de

just as outer workspace boundaries in traditional structures, as they cannot be crossed in specific configurations but there might be other IKS for which this boundary can be traversed on a nonsingular path. For offset wrist robots this poses a challenge, as the singularity set and its image are not easily described and therefore determining uniqueness domains, which in turn provide workspace regions in which the robot can freely move without the risk of reaching a singularity, remains an open problem.

Aiming to better understand such kinematic properties, we provide a method that simplifies the investigation of workspace regions of 6R manipulators and demonstrate it for two robots. It is based on the approach presented in Sect. 3 to reduce the 6-dimensional workspace to a 4-dimensional representation. In Sect. 4 we compute the number of IKS over the entire workspace to numerically detect critical values and study the behaviour of the robot there. We conclude in Sect. 5 with the potential and limitations of the presented work.

1.1 Related Work

Non-redundant robots that allow a nonsingular change of solutions are subject of numerous kinematic investigations [13]. They are said to be *cuspidal* and the 3R case is extensively studied, providing a starting point for the present work. In particular, [5] describes the commonly used 2 dimensional representation of Cartesian workspace for regional manipulators. We extend this notion to include orientational components. Uniqueness domains and smooth components of the critical value set are investigated in [12] for 3R architectures.

Due to the increased complexity, general results for non-anthropomorphic 6R designs are scarce. A collection of relevant results and conjectures is provided in [9]. In [11, 4], 16 analytical solutions to a specific pose are given for an offset wrist robot similar to the model investigated here and it is shown that this robot class can always perform a nonsingular solution change. An analysis of 6R robots with a range of variable DH parameters is described in [10], including an algorithm to check cuspidality as well as the repeatability of closed loops, which can be restrictive for such manipulators.

2 Preliminaries

The methods of this paper can be applied to any 6R manipulator. We demonstrate it on robots of the structure presented in Fig. 1. Notably, we allow an offset in the wrist given by a_5 or d_5. Without loss of generality, we require d_1, d_6 and a_6 to be zero. We will investigate two robots, one with $a_5 \neq 0$

i	d_i	a_i	α_i
1	0	0	$\frac{\pi}{2}$
2	0	a_2	0
3	0	0	$-\frac{\pi}{2}$
4	d_4	0	$\frac{\pi}{2}$
5	d_5	a_5	$-\frac{\pi}{2}$
6	0	0	0

(a)

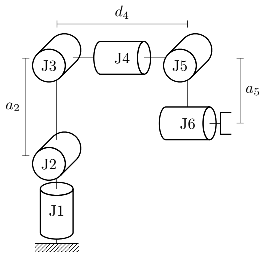

(b)

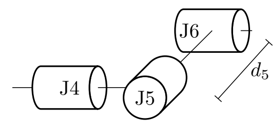

(c)

Fig. 1: The structure of the robots considered, with the non-zero DH-parameters listed in (a). *Robot T* with $a_5 \neq 0$ and $d_5 = 0$ is sketched in (b). The wrist of *Robot F* with $d_5 \neq 0$ and $a_5 = 0$ is shown in (c).

and $d_5 = 0$, named *Robot T*, and in Sect. 4.3 we compare it to *Robot F*, which has $d_5 \neq 0$ and $a_5 = 0$. The specific values are $a_2 = d_4 = 540$ and the non-zero value a_5 or d_5 is set to 150. *Robot T* is similar to the robot in [4] and commercial models of this type include the Agile Thor series and the discontinued KUKA Transpressor. The lengths are chosen such that *Robot F* coincides with the Fanuc CRX-10iA, which is shown to be cuspidal in [10].

By $f : \mathcal{J} \to \mathcal{W}$ we denote the forward kinematic map from the torus $\mathcal{J} = (S^1)^6$ to the special Euclidean group $\mathcal{W} = SE(3)$. With $\mathcal{S} \subset \mathcal{J}$ we denote the singular set and its image $f(\mathcal{S})$ is the set of critical values. *Uniqueness domains* are subsets $\mathcal{U} \subset \mathcal{J}$ such that the restriction of the forward kinematic map $f|_{\mathcal{U}}$ is injective. In other words, for any target we can find at most one IKS in $\mathcal{U}$. In particular, this means that we can follow any path in the image $f(\mathcal{U})$ with configurations in $\mathcal{U}$. For our purposes, we will always assume uniqueness domains to not contain any singularities and to be connected in $\mathcal{J}$.

Remark 1 Critical value sets of codimension greater than 1 cannot be detected by the numerical approach of Sect. 4. Such sets do not separate the workspace, meaning any path in $\mathcal{W}$ crossing it can be perturbed infinitesimally to avoid the singularity.[1] For wrist partitioned robots, this includes the set of wrist singularities. Even though this set has codimension 1 in $\mathcal{J}$, its image has codimension 2. From now on, when we mention singularities or critical values, we will always refer to the workspace separating type only.

[1] Of course, for path planning it might be sensible to avoid them with a reasonable distance, e.g., to avoid unnecessary joint accelerations.

3 Dimension Reduction of the Workspace

Since the space $SE(3)$ is 6-dimensional, workspace boundaries and codimension 1 critical value sets are 5-dimensional. As the analysis of such spaces is challenging, we propose a reduction by two dimensions which retains important kinematic properties. We make two assumptions on the world and end-effector frame: (1) The end-effector frame T_E coincides with the sixth joint, aligning the joint axis with the z-axis of T_E, and (2) the first joint axis coincides with the world z-axis.

We will leverage that the kinematic properties we are interested in, namely the number of IKS and singularities, are not affected by the first or last joint values. Thus, for the orientational component, it suffices to regard the direction of the last joint axis, omitting the rotation about joint 6. By assumption (1), the last joint axis coincides with the z-axis of the end-effector pose and we can extract its direction as the last column of the corresponding rotation matrix. This lies on a two dimensional manifold, namely a 2-sphere. Its points can be described by two angles (ϕ, ψ), which can be thought of the first two Euler angles for a suitable order of rotation axes, such as $z - x - z$.

For the positional component, we proceed as in the 3R case [5, 13] and leverage cylindrical coordinates to project $(x, y, z) \in \mathbb{R}^3$ to $(\rho, z) \in \mathbb{R}_{\geq 0} \times \mathbb{R}$ with $\rho^2 = x^2 + y^2$. This makes use of assumption (2).

Unfortunately, the orientational component still depends on the x and y values: If we rotate about the first joint (i.e., changing x and y while keeping ρ constant), the target joint axis will change direction with respect to the world coordinate system. To avoid this, consider an end effector pose with positional part $p = (p_x, p_y, p_z)$. With respect to p we define a modified reference frame T_p, obtained from the world coordinate system by rotating about the z_{world}-axis, aligning the x-axis of T_p with the vector $(p_x, p_y, 0)$. The angle of rotation γ is given by $\cos\gamma = p_x/\rho$ and $\sin\gamma = p_y/\rho$, provided $\rho \neq 0$. We define the pair (α, β) as the first two Euler angles considered with respect to the reference frame T_p. They relate to the previous angles by $(\alpha, \beta) = (\phi - \gamma, \psi)$.

Therefore the forward kinematics map can be represented by a mapping between 4-dimensional spaces, sending joint values $(\theta_2, \theta_3, \theta_4, \theta_5)$ to the corresponding end-effector coordinates (ρ, z, α, β).

4 Workspace Investigation

4.1 Clustering by the Number of IKS

To quantitatively evaluate the robots reach possibilities, we apply the above method and linearly sample the workspace over the four variables. Explicitly, we take $\alpha \in [0, 2\pi]$ and $\beta \in [0, \pi]$, which covers the entire sphere.[2] The values ρ and z are taken in the interval $[0, r_{max}]$, where r_{max} is the maximum reach of the robot. Due to symmetry in the robot kinematic, the positive values of ρ and z suffice to describe the entire workspace.

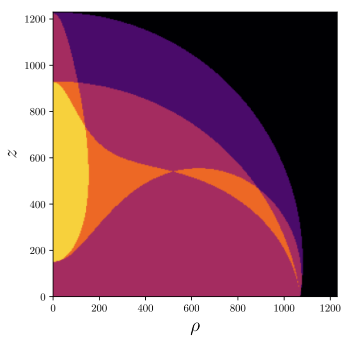

(a)

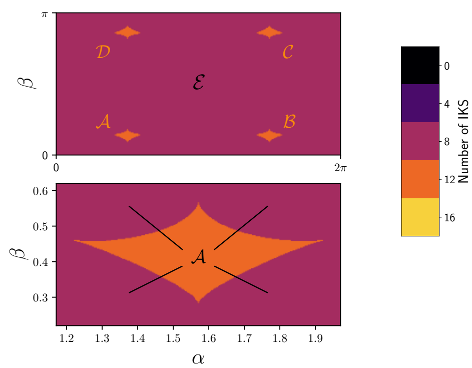

(b)

Fig. 2: (a) Number of solutions in coordinates (ρ, z) with fixed orientation $(\alpha, \beta) = (\pi/2, \pi/2)$ and $\rho, z \geq 0$ is shown. In (b) the coordinates are (α, β) and the position $(\rho, z) = (480, 0)$ is fixed. The upper plot shows all four regions with 12 IKS, while the lower plot is zoomed into $\mathcal{A}$ and the four boundary crossings are indicated. There exists one connected region $\mathcal{E}$ with 8 IKS.

For each sampled workspace point, we compute the number of IKS using the method of [4], but approaches as in [3, 6] could be used as well. The number of solutions is visualised as 2-dimensional slices with either the positional or rotational arguments fixed (Fig. 2). We encourage the reader to explore this further with the interactive variant and animations provided online (https://github.com/fea38135/ARK26_workspace). It is notable that for both robots the number of IKS appear only as multiples of 4, which is likely due to an invariance of the kinematic map described as *shoulder flip* in [4].

We can separate workspace into connected components with constant number of IKS. Within each component, the map f is a local isomorphism. In particular, for any two end effector poses in the same component one can find a unique one-to-one correspondence between the two sets of IKS. At the boundaries of these components are the critical values of the f.[3] At least one

[2] It is even a coordinate chart for $\alpha \neq 2\pi$, $\beta \neq 0, \pi$.

[3] As mentioned in Remark 1, there are likely critical value sets of lower dimension that are not detected by this approach.

joint configuration in the preimage of a critical value is singular. Since this might not be true for all IKS, we study the possibility of a nonsingular boundary crossing from all solutions by defining a linear path in $\mathcal{W}$ transversal to the boundary and tracing it for each IKS via Newton's method. It suffices to check one path crossing each smooth boundary component, as within the smooth components the behaviour remains the same. These boundaries were labelled *characteristic surfaces* in [12].

4.2 Classification of Configurations in a Workspace Region

We now restrict to the workspace region $\widetilde{\mathcal{W}}$ given by $\rho > 300$, $z < 750$, and arbitrary orientation. For *Robot T*, we provide a classification of configurations and describe corresponding uniqueness domains in $\widetilde{\mathcal{W}}$. The number of components with constant number of IKS in this region is rather small and therefore it is possible to individually check all crossings of critical values. Still, it is a reasonably large area and sufficient for many real-world applications. Moreover, this region will be suitable to emphasize differences in the comparison of Sect. 4.3.

Within $\widetilde{\mathcal{W}}$ there is one region $\mathcal{F}$ with 4 IKS, one region $\mathcal{E}$ with 8 IKS and four regions $\mathcal{A}, \mathcal{B}, \mathcal{C}$ and $\mathcal{D}$ with 12 IKS. The boundary between $\mathcal{E}$ and $\mathcal{F}$ has only one smooth component, where 4 of the 12 IKS merge in pairs, leaving 8 IKS in the adjacent region. Similar behaviour is generally expected at such boundaries as described in [7]. The crossings between the 12 IKS regions and $\mathcal{E}$ are more interesting and consist of 4 smooth components for each of the four regions which can be best seen in the orientational components of Fig. 2b.

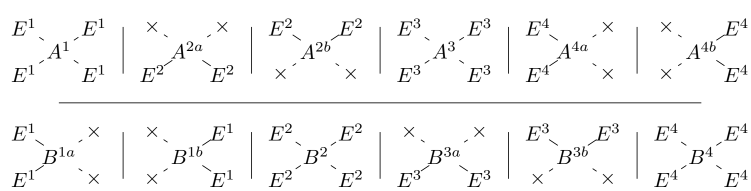

Fig. 3: Correspondence between the solutions for $\mathcal{E}$ and $\mathcal{A}, \mathcal{B}$ when crossing the 4 boundary components indicated in Fig. 2b. The symbol $\times$ indicates that the path ends in a singularity. We only show the first 6 (or 4) solutions in $\mathcal{A}, \mathcal{B}$ (resp. $\mathcal{E}$) as the second half follows the same pattern. Explicitly, the correspondence looks identical if we shift each index to the IKS from k to $k+4$. Moreover, the solutions of $\mathcal{C}$ (and $\mathcal{D}$) show the same pattern as the ones of $\mathcal{A}$ (resp. $\mathcal{B}$).

We describe $f^{-1}(\mathcal{E})$ as the disjoint union of solution regions $E^k, 1 \leq k \leq 8$, each mapping isomorphically to $\mathcal{E}$.[4] For the components of $f^{-1}(\mathcal{A})$ we use the suggestive notation $A^{kx}, 1 \leq k \leq 8$, where $x \in \{a, b\}$ is added for some of the k to distinguish all 12 solutions. Fig. 3 shows the correspondence of solutions when crossing the boundaries as indicated in Fig. 2b and reveals the motivation to this notation. The solution E^1 connects only to A^1, while E^2 connects to A^{2a} and A^{2b}. On the other hand, each solution A^{kx} is connected to exactly one solution region E^k, either via all 4 boundary components or by 2 adjacent components while the other 2 describe singularities. One proceeds similarly for $\mathcal{B}, \mathcal{C}$ and $\mathcal{D}$.

Note that singularities at these boundaries only appear starting from a 12 IKS region, as we generally expect a singularity to manifest as the merger of a pair of solutions. Moreover, starting with any solution E^k there is no nonsingular path to another solution for $\mathcal{E}$ without leaving $\widetilde{\mathcal{W}}$. Still, we can reach all of $\widetilde{\mathcal{W}}$ (up to the outer workspace boundary) from any of the 8 solutions E^k.

One has to take care when crossing into the 12 IKS regions from $\mathcal{E}$, as it is possible to reach different solutions there. As mentioned above, starting at E^2 we can end up either in A^{2a} or A^{2b}, depending on the boundary component crossed. Thus a nonsingular change of solutions is possible from A^{2a} to A^{2b}. Trying to cross to $\mathcal{E}$ from A^{2a} or A^{2b} through a part of the boundary not leading to E^2 ends in a singularity, i.e., interior workspace boundary. Denoting by ∂_n the nonsingular crossings between E^2 and A^{2x}, the union $U = E^2 \cup \partial_n \cup A^{2x}$ is a uniqueness domain for $x \in \{a, b\}$. But we just observed that there are boundary segments not in ∂_n that separate U locally, and cannot be crossed directly.

It is notable that all boundary crossings are possible if a suitable configuration is selected. For $\mathcal{A}$ this can be achieved with E^k and A^k for $k \in \{1, 3, 5, 7\}$ as they share no singular boundary. For these k, $E^k \cup \partial_n \cup A^k$ is a uniqueness domain with ∂_n including the entire boundary. Unfortunately, this cannot be extended to all of $\widetilde{\mathcal{W}}$. We can include $\mathcal{C}$ and its boundaries for these IKS, but they can reach singular values after crossing into $\mathcal{B}$ or $\mathcal{D}$. Thus we can enlarge our uniqueness domain to $E^k \cup A^k \cup B^{kx} \cup C^k \cup D^{ky} \cup \partial_n$ with $k \in \{1, 3, 5, 7\}$ and $x, y \in \{a, b\}$. But we cannot select any combination such that ∂_n includes all boundary components for B^{kx} and D^{ky}. For the other values of k we can include all boundaries of $\mathcal{B}$ and $\mathcal{D}$ but only some for $\mathcal{A}$ and $\mathcal{C}$.

This shows that with offset wrist robots, it is possible to obtain a large workspace area, where under suitable configuration selection any end-effector path can be traced without running into singularities. But one cannot expect to expand the workspace arbitrarily, as we demonstrated even in the region $\widetilde{\mathcal{W}}$.

---

[4] Again, one might need to remove nonseparating critical value sets.

Note that outside $\widetilde{\mathcal{W}}$ there exist nonsingular paths between some of the 8 solutions in $\mathcal{E}$, one can check this by regarding piecewise linear motions (in jointspace) between the IKS at suitable targets as in [4].

4.3 Comparison of Two Wrist Offset Structures

To show how a different robot structure effects the motion capabilities, we present some results for *Robot F*. The complexity of the singularity and critical value sets is increased, which could be already expected from the fact, that the Jacobian determinant for *Robot T* has two factors while for *Robot F* it usually does not factor. In the workspace visualisation this results in more complex patterns for the regions with constant number of IKS. For an area similar to $\widetilde{\mathcal{W}}$, many more crossings would have to be checked.

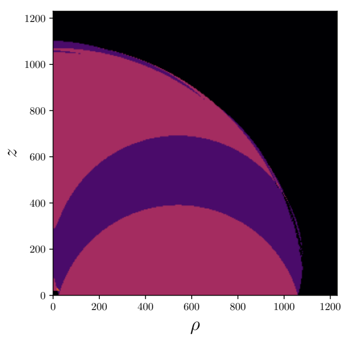

(a)

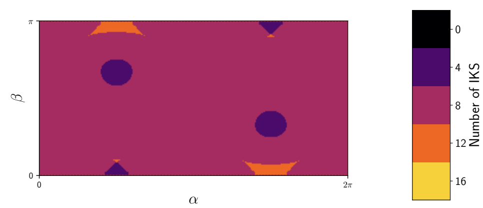

(b)

Fig. 4: Number of solutions for *Robot F*, where in (a) we fixed $(\alpha, \beta) = (\pi/2, \pi/2)$, and for (b) we set $(\rho, z) = (475, 260)$.

When fixing $\alpha = \pi/2$ and $\beta = \pi/2$, i.e., the last joint axis oriented orthogonally away from z_{world} the resulting slice is shown in Fig. 4a. Here, a 4 IKS region separates Cartesian workspace, meaning Cartesian motions with this fixed orientation are limited for the 4 solutions vanishing there. Similarly to *Robot T*, when changing the orientation we have the other 4 solutions vanishing, preventing an "optimal" choice in configuration. These 4 IKS regions are in addition to 12 IKS regions, which show similar behaviour as in the first case.

5 Consequences and Outlook

Determining uniqueness domains for 6R robots with offset wrists is fundamental to find workspace regions with unrestricted motion possibilities. Since both orientational and positional components have to be considered, the described reduction to a 4-dimensional representation of the workspace provides a powerful tool to investigate and visualize properties of 6R robots. Still, even for restricted workspace regions the description of uniqueness domains requires careful study. But they provide crucial information about the robots motion capabilities. We demonstrated that one cannot expect to find ”optimal” uniqueness domains for offset wrist robots. One has to prioritise in which workspace region unrestricted motion capabilities are required and where limitations are acceptable.

Therefore, this should be taken into consideration in the development process of such robots. For users requiring precise motions planning in workspace, we recommend determining a workspace region that suffices for the tasks in mind and analysing critical values there to determine problematic areas.

The main drawback of the method described is the required manual separation of smooth boundary components. This is cumbersome and prone to errors, and one might not detect some components at all, e.g., due to limited resolution. An exact representation for the smooth components of the critical value set would be ideal, but no such result is known to the authors. Improvements might be achieved by increasing the sampling resolution, e.g., with a marching hypercubes technique [1], and by algorithmically checking nonsingular connectivity using algebraic methods [2].

References

1. Castelo, A., Moutinho Bueno, L., Gameiro, M.: A combinatorial marching hypercubes algorithm. Computers & Graphics **102**, 67–77 (2022)
2. Cummings, J., Hauenstein, J.D., Hong, H., Smyth, C.D.: Smooth connectivity in real algebraic varieties. Numerical Algorithms **100**(1), 63–84 (2025)
3. Elias, A.J., Wen, J.T.: IK-geo: Unified robot inverse kinematics using subproblem decomposition. Mechanism and Machine Theory **209**, 105,971 (2025)
4. Feeß A.; Weiß, M.G.: Analysis of a cuspidal 6R robot. In: Proceedings of the 3rd IMA Conference on Mathematics of Robotics (to appear 2026)
5. Husty, M., Ottaviano, E., Ceccarelli, M.: A geometrical characterization of workspace singularities in 3R manipulators. In: Advances in Robot Kinematics: Analysis and Design, pp. 411–418. Springer (2008)
6. Husty, M.L., Pfurner, M., Schröcker, H.P.: A new and efficient algorithm for the inverse kinematics of a general serial 6R manipulator. Mechanism and Machine Theory **42**(1), 66–81 (2007)
7. Kohli, D., Spanos, J.: Workspace Analysis of Mechanical Manipulators Using Polynomial Discriminants. Journal of Mechanisms, Transmissions, and Automation in Design **107**(2), 209–215 (1985)

8. Pieper, D.L.: The kinematics of manipulators under computer control. Ph.D. thesis, Stanford University (1969)
9. Salunkhe, D.H.: Cuspidal robots : Theoretical study, classification, and application to commercial robots. Ph.D. thesis, École centrale de Nantes (2023)
10. Salunkhe, D.H., Marauli, T., Müller, A., Chablat, D., Wenger, P.: Kinematic issues in 6R cuspidal robots, guidelines for path planning and deciding cuspidality. The International Journal of Robotics Research **44**(6), 1035–1054 (2025)
11. Weiß, M.G.: A class of 6R robots and poses with 16 analytical solutions. In: Proceedings of the IMA Conference on Mathematics of Robotics (2015)
12. Wenger, P.: Uniqueness domains and regions of feasible paths for cuspidal manipulators. IEEE Transactions on Robotics **20**(4), 745–750 (2004)
13. Wenger, P., Chablat, D.: A review of cuspidal serial and parallel manipulators. Journal of Mechanisms and Robotics, American Society of Mechanical Engineers **15**(4), 1–37 (2022). DOI 10.1115/1.4055677